# Fast spatial scanning of 3D ultrasound fields via thermography

K. Melde,[1] T. Qiu,[1] and P. Fischer[1,2,a)]
[1]Max Planck Institute for Intelligent Systems, Heisenbergstr. 3, 70569 Stuttgart, Germany
[2]Institut für Physikalische Chemie, Universität Stuttgart, Pfaffenwaldring 55, 70569 Stuttgart, Germany

(Received 2 July 2018; accepted 7 September 2018; published online 26 September 2018)

We propose and demonstrate a thermographic method that allows rapid scanning of ultrasound fields in a volume to yield 3D maps of the sound intensity. A thin sound-absorbing membrane is continuously translated through a volume of interest while a thermal camera records the evolution of its surface temperature. The temperature rise is a function of the absorbed sound intensity, such that the thermal image sequence can be combined to reveal the sound intensity distribution in the traversed volume. We demonstrate the mapping of ultrasound fields, which is several orders of magnitude faster than scanning with a hydrophone. Our results are in very good agreement with theoretical simulations. *Published by AIP Publishing*. https://doi.org/10.1063/1.5046834

Ultrasound fields are used both for imaging and to inspect and interact with matter.[1–3] This often requires focused or shaped beams. For instance, in the manipulation of particles or cells, it is vital that the exact beam shape is known.[4,5] Therapeutic and medical applications further require the knowledge about hotspots, points of unwanted high pressure amplitude, outside of the therapeutic region.[6–8] Conventionally, underwater ultrasound fields are mapped by scanning a hydrophone through the region of interest. While this provides amplitude and phase information, it is extremely slow and therefore of limited use to acquire 3D fields. Emerging technologies for field synthesis and dynamic applications of ultrasound would benefit from a faster method to obtain volumetric information of the sound pressure.

A calibrated hydrophone allows both pressure amplitude and the complex phase to be measured with a high degree of accuracy, but only at a point. Its size is determined by the aperture of the hydrophone and often chosen to be smaller than the wavelength of the measured acoustic field. At larger aperture sizes, the hydrophone tip cannot be considered a point. The measured field is then a function of the tip geometry and the amplitude distribution across its aperture and exact phase measurements become impossible. To acquire a spatial distribution, the hydrophone has to be scanned through a set of points, a process that does not scale well to large areas or volumes. Typical acquisition rates are on the order of 1 voxel per second, resulting in multiple hours or even days for a full scan.[9] Furthermore, long scanning times may result in drift errors due to changes in the environment or transducer, i.e., caused by temperature changes or evaporation of liquid. The conventional solution to reduce the measurement time, e.g., for simple fields that only provide a single focus, is to limit the scan to orthogonal planes that cut through the center of the focal spot.[10] Ideally, one precision measurement in a transverse plane to the wave propagation direction is sufficient to compute the whole 3D field by virtual wave propagation.[11] This, however, can produce significant artifacts if the initial complex valued sound field contains measurement errors.[12]

Alternative approaches rely on the acousto-optical effect, which depends on the change of the optical refractive index as a function of the density (pressure) of the traversed medium. The effect is for instance employed in two-dimensional Fabry-Perot sensors. The acoustic pressure changes the optical density between two parallel, reflecting surfaces of a thin film, which in turn can be detected by a scanning laser.[9,13] Another acousto-optical technique is schlieren imaging, where a collimated beam of light passes through an ultrasound field and diffracts where the index of refraction is changed due to the pressure field. A camera is positioned behind a knife edge or patch stop that blocks the undiffracted light. Only higher order diffracted light will reach the sensor, which results in a 2D projection of the density variation in the measurement volume. By rotating the transducer, one can take recordings at different angles and reconstruct the volumetric data using the inverse Radon transform.[14,15] Similar results can be obtained from laser Doppler velocimetry, where a (scanned) laser beam interrogates a target after passing through the region of interest. Contrary to typical velocimetry measurements, the target does not move but instead the variations of the refractive index in the region of interest change the effective optical path length, which can in turn be used to infer the properties of the acoustic field.[16] Difficulties arise for high amplitude sound fields when the optical phase difference in the field of view exceeds $2\pi$.[17] Acousto-optic methods require optical access, long working distances, and specialized setups, unlike the method we present herein.

Direct and immediate visualization of a sound field can be very useful in the lab. A simple method uses the thermochromic effect of liquid crystals.[18] A temperature change induces phase changes in the liquid crystal, which results in a visible color change. Coating of a sheet containing thermochromic liquid crystals with a thin sound absorbing layer causes it to display a spatial color distribution related to the locally absorbed sound intensity. This concept has been used to map 3D sound fields in conjunction with a camera.[19,20] While the method is extremely simple and permits direct and instantaneous information, the color calibration is not trivial

a)Author to whom correspondence should be addressed: fischer@is.mpg.de

and the temperature (and pressure) measurement range is limited depending on the liquid crystal material.[21]

In this Letter, we present a high resolution thermographic method to rapidly measure 3D sound fields by recording the surface temperature across a sound-absorbing membrane with a standard thermal camera. A schematic of the setup and the data analysis is displayed in Fig. 1. In this case, a transducer is submerged in a water tank and points upwards. The measurement device is an open cylindrical cup with a thin membrane forming the bottom surface, which is made of a sound absorbing material. A thermal camera is mounted at a fixed distance from the membrane. An automated stage translates camera and membrane through the region of interest along the z-coordinate. The cup ensures that the top surface of the membrane is always exposed to air and allows direct viewing by the camera. When the sound field is turned on, it propagates through the liquid, reaches the membrane, and then partially couples into the membrane where it is absorbed. This causes a local temperature rise at the surface of the membrane, which is detected by the camera. Each camera image shows the temperature distribution in a whole plane (XY). By moving the cup and membrane with a known speed while recording a sequence of thermal images, we can construct a 3D volume distribution of the recorded temperature maps, which in turn indicate the absorbed sound intensity. Calibration of the membrane and camera allows us to estimate the sound pressure amplitude in the same volume. In this work, we show how to acquire a volume map of $3\,\text{cm} \times 3\,\text{cm} \times 6\,\text{cm}$ (containing more than $6 \times 10^6$ voxels) in just 33 s. Our technique thereby allows us to quickly validate the spatial structure of complex sound fields.

The performance of the thermographic method depends on process parameters including the thermal and mechanical properties of the absorbing membrane and its thickness, the scanning speed, and the thermal camera. A simplified geometry is displayed in Fig. 2(a) for a material with acoustic attenuation coefficient $\alpha$, heat conductivity $k$, and specific heat capacity $C_p$. The top surface is exposed to air while the bottom surface is in contact with the water bath at room temperature. Coupling of an acoustic wave into a thin material layer depends on its mechanical properties in contrast to the liquid medium and its thickness in relation to the wavelength $\lambda$. Shown in Fig. 2(b) is the coupling coefficient $\gamma$, which relates the incident to the transmitted (and therefore lost) sound intensity into a membrane of thickness $H$. Its derivation can be found in the supplementary material. As expected, a thicker membrane absorbs more total power with distinct peaks corresponding to multiples of half the wavelength. The remaining sound intensity, which is reflected, will travel further through the setup and may return to the membrane after another reflection. The most likely case is reflection off the transducer surface. This will introduce systematic errors that depend on the distance between the membrane and the transducer. The ideal membrane exhibits a coupling factor of $\gamma = 1$.

The heating of a material due to attenuation of a plane travelling sound wave is $q = -\nabla I_2 = 2\alpha_2 \langle p_2^2 \rangle / \rho_2 c_2$,[22] where $I$ and $p$ are the sound intensity and pressure, $\rho$ the density, and $c$ the speed of sound. The brackets denote a time average. In this work, subscripts 1 or 2 refer to quantities in the water or membrane domain, respectively. In the absence of precise,

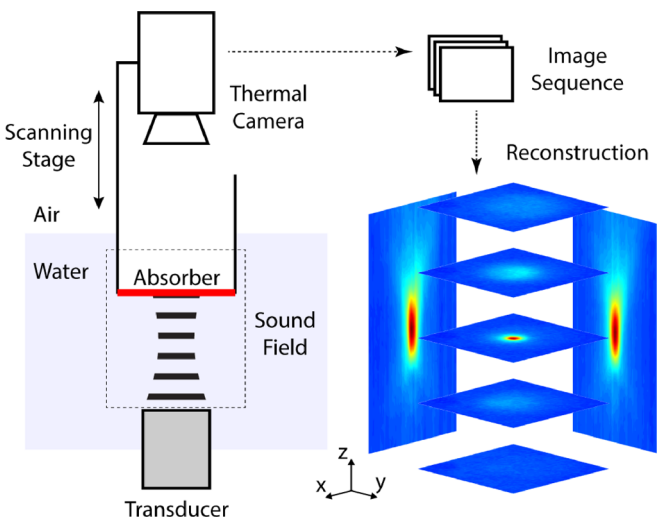


FIG. 1. Schematic and workflow. A membrane made of ultrasound absorbing material is locally heated by the sound field. This temperature change is detected by a thermal camera, which is mounted at a fixed distance from the membrane. Continuous scanning of the assembly along the z-direction with the transducer turned on produces a sequence of thermal images that allows reconstruction of the ultrasound field in all 3 dimensions. Shown are exemplary XY-planes and projections of the central XZ- and YZ-plane.

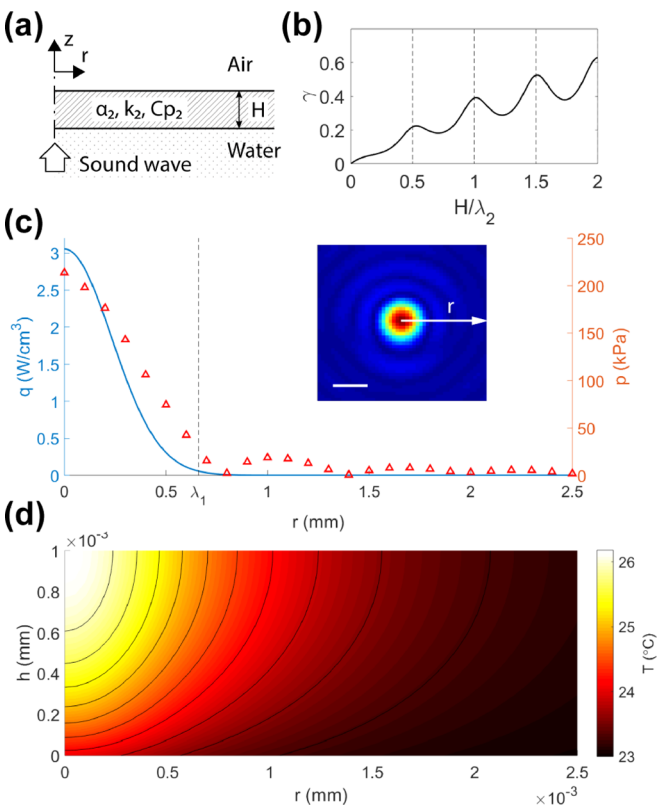


FIG. 2. Thermal signal response of a sound absorbing membrane. (a) Axially symmetric geometry used for simulations with dimensions and material parameters. (b) Coupling coefficient $\gamma$ for sound transmission from water into a membrane of thickness $H$ and $c_2 = 1800\,\text{m s}^{-1}$, $\rho_2 = 1100\,\text{kg m}^{-3}$. Dashed lines mark multiples of $\lambda_2/2$. (c) Heat input $q$ for the simulation derived from an exemplary measured single focal point. Its peak is aligned with the origin ($r = 0$ mm). Scale bar: 1 mm. (d) Steady state temperature distribution in the cross-section of a virtual rubber material with $H = 1$ mm.

published data regarding the materials, we assume typical values for a general elastomer material with the parameters $k_2 = 0.2\ W\,m^{-1}\,K^{-1}$, $C_{p2} = 1900\ J\,kg^{-1}\,K^{-1}$, $c_2 = 1800\ m\,s^{-1}$, $\rho_2 = 1110\ kg\,m^{-3}$, and $\alpha_2 = 10\ dB\,cm^{-1}$, which are obtained from reported isobutyl rubber values.[23,24] The corresponding model is implemented in Matlab (MathWorks Inc., USA) using the Partial Differential Equation Toolbox. The input to our simulations is a heating function $q$ described by a Gaussian distribution with a waist size based on a measured focus. The corresponding hydrophone scan is shown as an inset to Fig. 2(c), and the sound pressure along the coordinate $r$ is plotted in the graph for comparison. Using this model, we can compute transient and steady state solutions to this problem. One exemplary steady state temperature distribution for a 1 mm thick rubber material can be seen in Fig. 2(d). The spot size at the top surface scales linearly with the membrane thickness $H$. This is expected for a membrane with isotropic heat conduction that is mainly cooled by convection of the water at the bottom surface. The ideal membrane is therefore thin and perfectly absorbing. We fabricated membranes from two different rubber materials for comparison with our simulations. The first material is an isobutyl rubber (IIR, Reichelt Chemietechnik GmbH + Co., Germany) with a thickness of 1.0 mm and the same material parameters as the ones we have assumed (*vide supra*) for our calculations. The second material is optimized for ultrasound absorption in the lower MHz range and available as a two-component fluid (Aptflex F36, Precision Acoustics Ltd., UK), which contains scattering particles embedded in a soft polyurethane matrix. The attenuation factor is $\alpha_2 = 30\ dB\,cm^{-1}\,MHz^{-1}$, and the other material parameters are approximately $k_2 < 0.3\ W\,m^{-1}\,K^{-1}$, $c_2 = 1500\ m\,s^{-1}$, and $\rho_2 = 1060\ kg\,m^{-3}$. We cured thin films of Aptflex F36 on a 0.1 mm thick polyethylene sheet to provide mechanical stability. The total thickness of both layers was then measured to be $0.43 \pm 0.02$ mm using a digital microscope (VHX-6000, Keyence, Osaka, Japan). At our operating frequency of 2.25 MHz, the coupling coefficients $\gamma$ are 0.3 for the IIR and 0.4 for the Aptflex membrane.

Figure 3(a) shows the steady state temperature on the surface versus recorded peak pressure of a single focal spot. In the experiment, the focal spot is created by a large area immersion transducer (A395S, Olympus Scientific Solutions Americas Inc., USA) with an operating frequency of 2.25 MHz, a diameter of 38.1 mm, and a focusing phase plate (focal length f = 30 mm). The transducer is located in the center of an open-topped water tank with the dimensions 600 mm (length) × 300 mm (width) × 300 mm (height) and positioned pointing up. The sides and bottom of the tank are lined with ultrasound attenuating sheets made of 10 mm thick Aptflex F28 (Precision Acoustics Ltd., UK). We first measured the peak sound pressure in the focus as a function of the driving voltage using a calibrated needle hydrophone (aperture diameter 0.5 mm $< \lambda_1$, sensitivity 545 mV MPa$^{-1}$ at 2 MHz, Precision Acoustics Ltd., UK). In a second experiment, we used the thermography setup to record the steady state temperature in the same focus versus the driving voltage. The two measurement results are combined and displayed in the chart of Fig. 3(a). For comparison, we ran the simulation for the general elastomer material for the two thicknesses and varying attenuation coefficients. The data clearly show the expected quadratic dependence between temperature and sound pressure. These experimental curves serve as calibration data to recover the sound pressure amplitude from the scanned temperature profiles. To quantify the noise, we evaluated the recorded temperature of single pixels over a 5 s range just before the ultrasound exposure started and adopted the noise equivalent pressure (NEP) method of Martin *et al.*[9] Three times the standard deviation was found to be approximately 0.1 °C for all recordings, which corresponds to an NEP of 23.6 kPa for Aptflex and 34.1 kPa for the IIR rubber. For comparison, the broadband noise (100 MHz) of the hydrophone system is rated at 60 $\mu$V by the manufacturer leading to an NEP of 330 Pa. In conjunction with a lock-in amplifier at 2.25 MHz (input range set to 200 mV, i.e., 367 kPa), we measured an NEP of 1.6 Pa. Thermography is therefore not as sensitive or accurate as a hydrophone measurement but rather a convenient tool for rapid spatial mapping of acoustic fields in 3D.

To characterize the dynamic performance of the system, we have recorded the time response of both membrane materials to a step input in the same setup as for the steady state measurements. The curves are shown in Fig. 3(b). When the transducer is turned on, the surface temperature in the spot quickly rises and then slowly converges to a steady state with the time constant $\tau$. From first principles, this time constant is approximately $\tau \approx \rho_2 C_{p2} H^2 / k_2$.[25] This quantity

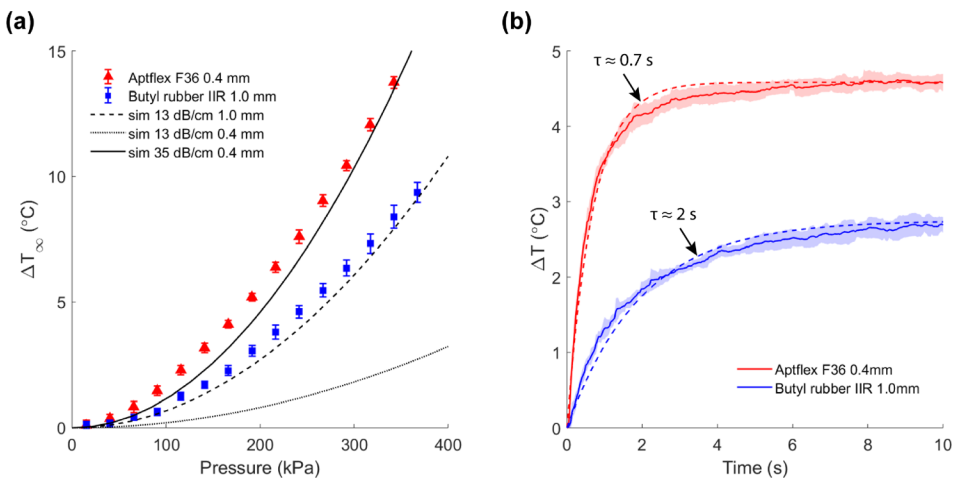


FIG. 3. (a) Steady state peak temperature plotted against peak pressure in the focus. (b) Average step response curves from 5 recordings per material (solid lines—mean, shaded regions—one standard deviation). Dashed lines show fits of exponential functions to the data and their respective time constants are annotated.

should be minimized to improve the response time and therefore the spatial accuracy when continuous scanning is used. The plot also shows the fitted exponential functions and associated time constants: 2.0 s for the IIR rubber and 0.7 s for the Aptflex membrane. Those time constants span several million cycles of ultrasound in the MHz range, which makes this metrology more useful for continuous wave fields. The optimal conditions of low $\tau$ and high $\alpha$ suggest that thin membranes made from highly absorbing materials perform better for the thermographic recording of ultrasound fields.

The distance between the thermal camera (A65, FLIR Systems Inc. USA) and the membrane in our setup is fixed to 200 mm. Using a calibration target, we found the lateral resolution in the thermal images to be 0.13 mm per pixel. The resolution in the scanning direction is $v_z/f_{\mathrm{cam}}$, where $v_z$ is the scanning speed and $f_{\mathrm{cam}}$ the frame rate of the camera. Typical values in our setup are $v_z = 1.8\,\mathrm{mm\,s^{-1}}$ and $f_{\mathrm{cam}} = 30\,\mathrm{s^{-1}}$, resulting in a z-resolution of 0.06 mm per pixel. The uncertainty following such a discretization is $\pm 1/2$ of the step size. Microbolometer detectors such as our thermal camera exhibit an impulse response to the IR signal, which the manufacturer reports as 12 ms in the datasheet. This is included in the earlier measured time constants. As a result, the dynamic response of the absorber distorts the signal in the z-direction according to an impulse response $g(z) = \frac{1}{\tau} e^{-z/\tau v_z}$. Figure 4 shows slices of measured temperature distributions for the better performing material and the sound field measured by a hydrophone. The thin and highly absorbing membrane gives a clear picture of the overall dimensions and location of the focal spot. Profile plots across the focal point ($x = 0$) are shown in Fig. 4(c). It is noticeable how the focus in the thermographic scan is extended along the positive y-axis. Following our analysis, there is a systematic error in the positive scanning direction that can be expressed as $\tau v_z = 0.7\,\mathrm{s} \times 1.8\mathrm{mm/s} = 1.26\,\mathrm{mm}$.

We finally demonstrate the method by imaging an unknown pressure field that we generate using a different phase plate, one that creates two foci (further called F1 and F2) at different z-depths as shown in Fig. 5(a). Using the calibration data from Fig. 3(a), we convert the change in temperature to a sound pressure amplitude. The result is displayed in Fig. 5(b), and the hydrophone scans around each region of interest can be found in supplementary material Fig. S2. The hydrophone measurement revealed peak pressures of 127 kPa (F1) and 122 kPa (F2). The peak pressure amplitudes acquired by the thermographic method with the Aptflex membrane are 115 kPa (F1) and 130 kPa (F2), where the variations are comparable to the NEP (23.6 kPa). The thermographic scan covered a total volume of 30 mm × 30 mm × 60 mm in about 33 s providing a rapid assessment of the 3D sound pressure field compared to conventional methods. Figure 5(c) illustrates volumetric information of the foci via pressure isosurfaces around each point.

In conclusion, we present a methodology to rapidly scan 3D volumes of ultrasound fields with a spatial resolution in the sub-millimeter range. The method relies on mechanically translating a thin absorbing sheet through a body of water while taking thermal images of the membrane, which is heated by the continuous ultrasound field. The thermal image stack is then converted to a volume pressure map. The

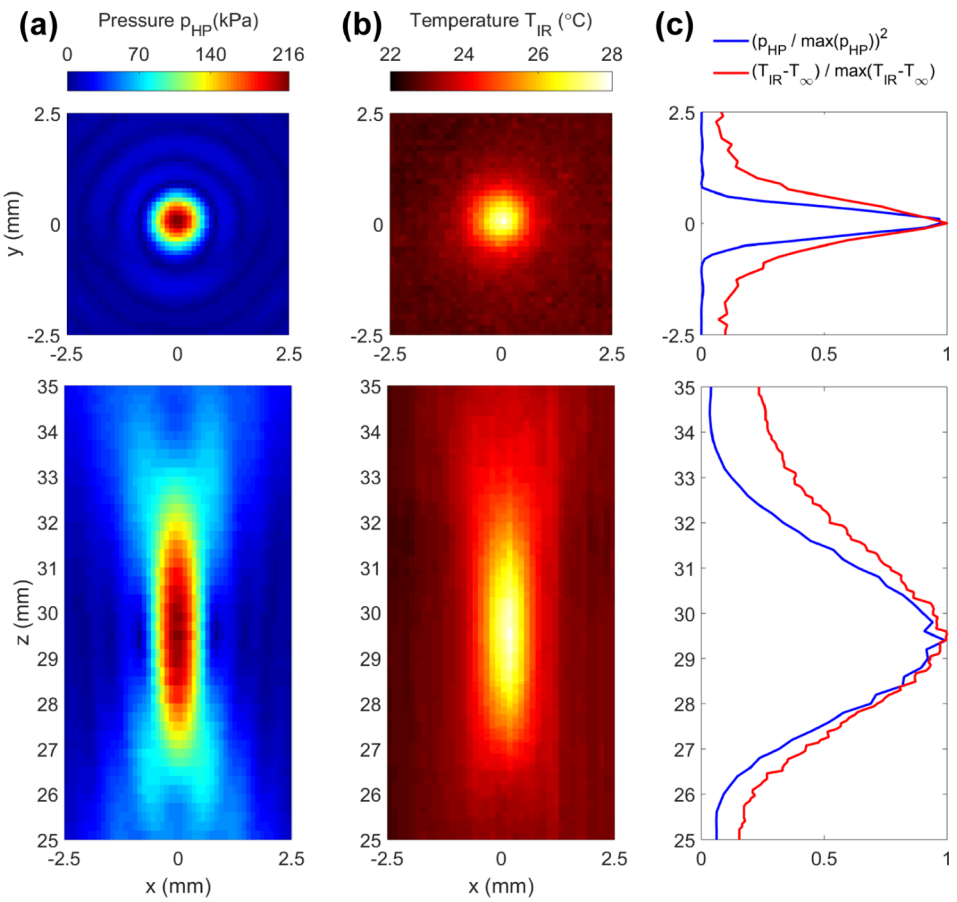


FIG. 4. Scans of an ultrasound focus at 2.25 MHz and transducer driving voltage $U_{TD} = 15\,V_{p\text{-}p}$. Displayed are slices through the focus, XY (top) and XZ (bottom). (a) Pressure amplitude from hydrophone measurement. (b) Recorded temperature distribution from a thermographic scan of the same field using a membrane made of 0.4 mm Aptflex F36 rubber ($\tau \approx 0.7$ s). Scanning velocity $v_z = 1.8\,\mathrm{mm\,s^{-1}}$. (c) Squared pressure and temperature profiles (along $x = 0$) normalized by their respective maximum values in the measurement. Room temperature $T_\infty = 22.1\,^\circ\mathrm{C}$.

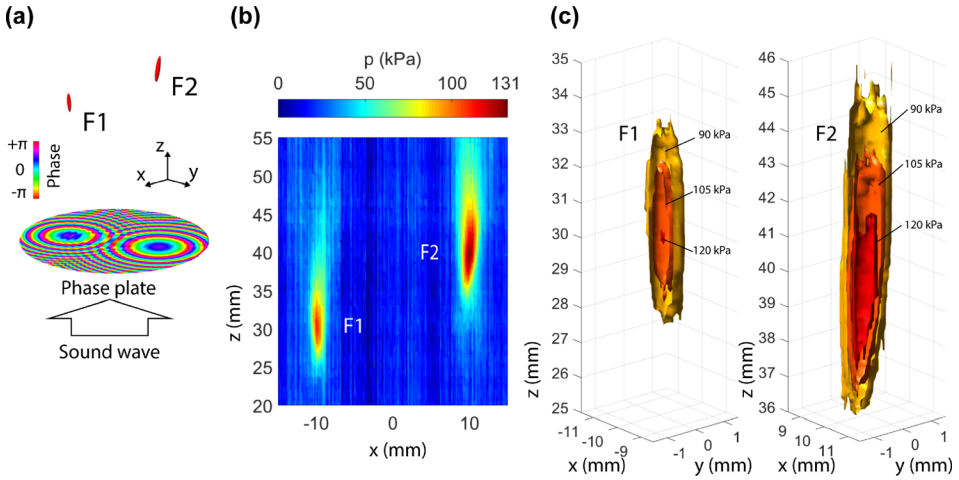


FIG. 5. (a) Phase plate for generating two foci F1 and F2. (b) Central slice ($y = 0$) of reconstructed pressure distribution from a thermographic scan. See supplementary material for hydrophone scans. (c) 3D isocontours of the focal regions from the reconstructed pressure distribution obtained from the thermographic data of (b).

sensitivity and precision of the method rely on and can be controlled by the characteristics of the film and its thickness, the scanning speed, and the resolution of the thermal imaging system. Using a thin ultrasound absorber sheet made from Aptflex F36 and polyethylene, we image a 3 cm × 3 cm area with $10^4$ pixels at a lateral resolution of 0.13 mm in 700 ms. Scanning the membrane in the third dimension allows us to map the volume of 54 $cm^3$ in 33 s. Our method is thus useful to obtain fast volume data on ultrasound pressure distributions and is orders of magnitude faster than hydrophone scanning. It is much simpler to implement than acousto-optical setups and does not require tomographic reconstruction. We expect that our method is useful in rapid visualization of complex structured ultrasound fields.

See supplementary material for a derivation of the coupling coefficient $\gamma$ and the hydrophone scans of the double foci experiment.

[1]G. ter Haar, Prog. Biophys. Mol. Biol. **93**(1–3), 111 (2007).
[2]M. R. Bailey, V. A. Khokhlova, O. A. Sapozhnikov, S. G. Kargl, and L. A. Crum, Acoust. Phys. **49**(4), 369 (2003).
[3]G. Harvey, A. Gachagan, and T. Mutasa, IEEE Trans. Ultrason. Ferroelectr. Freq. Control **61**(3), 481 (2014).
[4]A. Franklin, A. Marzo, R. Malkin, and B. W. Drinkwater, Appl. Phys. Lett. **111**(9), 094101 (2017).
[5]K. Melde, E. Choi, Z. Wu, S. Palagi, T. Qiu, and P. Fischer, Adv. Mater. **30**(3), 1704507 (2018).
[6]M. S. Canney, M. R. Bailey, L. A. Crum, V. A. Khokhlova, and O. A. Sapozhnikov, J. Acoust. Soc. Am. **124**(4), 2406 (2008).
[7]O. Naor, S. Krupa, and S. Shoham, J. Neural Eng. **13**(3), 031003 (2016).
[8]Y. Hertzberg and G. Navon, Med. Phys. **38**(12), 6407 (2011).
[9]E. Martin, E. Z. Zhang, J. A. Guggenheim, P. C. Beard, and B. E. Treeby, IEEE Trans. Ultrason. Ferroelectr. Freq. Control **64**(11), 1711 (2017).
[10]J. Seo, N. Koizumi, K. Yoshinaka, N. Sugita, A. Nomiya, Y. Homma, Y. Matsumoto, and M. Mitsuishi, IEEE Trans. Ultrason. Ferroelectr. Freq. Control **57**(4), 883 (2010).
[11]W. Kreider, P. V. Yuldashev, O. A. Sapozhnikov, N. Farr, A. Partanen, M. R. Bailey, and V. A. Khokhlova, IEEE Trans. Ultrason. Ferroelectr. Freq. Control **60**(8), 1683 (2013).
[12]O. A. Sapozhnikov, S. A. Tsysar, V. A. Khokhlova, and W. Kreider, J. Acoust. Soc. Am. **138**(3), 1515 (2015).
[13]E. Zhang, J. Laufer, and P. Beard, Appl. Opt. **47**(4), 561 (2008).
[14]Y. R. Jia, Q. Wei, D. J. Wu, Z. Xu, and X. J. Liu, Appl. Phys. Lett. **112**, 173501 (2018).
[15]S. Harigane, R. Miyasaka, S. Yoshizawa, and S. Umemura, Jpn. J. Appl. Phys. **52**, 07HF07 (2013).
[16]A. R. Harland, J. N. Petzing, and J. R. Tyrer, J. Acoust. Soc. Am. **115**(1), 187 (2004).
[17]T. Nakamura, R. Iwasaki, S. Yoshizawa, and S.-I. Umemura, Jpn. J. Appl. Phys., Part 2 **57**(7S1), 07LB13 (2018).
[18]K. Martin and R. Fernandez, Ultrasound Med. Biol. **23**(8), 1267 (1997).
[19]G. A. Lopez Munoz and G. A. Valentino Orozco, in *New Developments in Liquid Crystals*, edited by G. Tkachenko (IntechOpen, 2009).
[20]K. Melde, A. G. Mark, T. Qiu, and P. Fischer, Nature **537**(7621), 518 (2016).
[21]N. Abdullah, A. Abu Talib, A. A. Jaafar, M. A. M. Salleh, and W. T. Chong, Exp. Therm. Fluid Sci. **34**(8), 1089 (2010).
[22]F. P. Curra, P. D. Mourad, V. A. Khokhlova, R. O. Cleveland, and L. A. Crum, IEEE Trans. Ultrason. Ferroelectr. Freq. Control **47**(4), 1077 (2000).
[23]T. Bhowmick and S. Pattanayak, Cryogenics **30**(2), 116 (1990).
[24]M. Sinha and D. J. Buckley, in *Physical Properties of Polymers Handbook*, edited by J. E. Mark (Springer, New York, 2007), p. 1021.
[25]M. Necati Özışık, *Heat Conduction*, 2nd ed. (John Wiley & Sons, Inc., New York, 1993).